Supporting information New Journal of Chemistry

Green synthesis of orthorhombic Mn_2O_3 nanoparticles; influence of the oxygen vacancies on antimicrobial activities and cationic dye degradation

Prammitha Rajaram [a†], Ambrose Rejo Jeice[a*] Kumarasamy Jayakumar [b†]

[a]*Department of Physics and Research Centre, Annai Velankanni College, Tholayavattam - 629157, Kanyakumari District, Tamil Nadu-629157, India, Affiliation to Manonmanium Sundaranar University, Abishekapattai, Tirunelveli - 627 012, Tamilnadu, India.*

[b]*Institute of Functional Materials and Agricultural Applied Chemistry, Jiangxi Agricultural University, Nanchang 330045, P. R. China*

[†]These authors contributed equally

***Corresponding author**

E mail (rejojeice@gmail.com,)

Mobile No: +918807841121

S MATERIALS AND METHODS

S1 Materials

Manganese (II) acetate tetrahydrate [$(CH_3COO)_2Mn.4H_2O$, 99.5 %], acetone (C_3H_6O), distilled water, and *methylene blue* ($C_{16}H_{18}CIN_3S$) were obtained by Loba chemicals. All of the compounds were analytical-grade and can be utilized without any other filtration process. *Veldt grape* leaf (scientific name: *Cissus quadrangularis Linn*) was procured from the locality of Marthandam, Tamil Nadu, India. Microbial strains like *Proteus mirabilis* (*P. mirabilis*), *Aeromonas hydrophila* (A. hydrophila), and Aspergillus flavus (A. flavus) were employed to examine biological effects.

S2 Characterization

The absorption spectra of the as-synthesized Mn_2O_3 NPs were examined by a UV-Visible Spectrometer (Perkin Elmer, model-Lambda 35). The crystalline nature and phase structure were examined using an X-Ray Diffractometer (Shimadzu XRD 6000). The chemical composition of the Mn_2O_3 NPs was determined through a Fourier Transform Infrared Spectrometer (FTIR) (Perkin Elmer, model-spectrum two). Scanning Electron Microscopy (JEOL, model-JSM-639) and High-Resolution Transmission Electron Microscopy (JEOL, model-JSM 2100) were used to analyze the Mn_2O_3 NPs' surface morphology. Utilizing an external scientific instrument known as the X-probe, X-Ray000 400um-FG ON (400 m), X-ray photon spectroscopic was used to study the functional compounds that comprise manganese (Mn 2p), oxygen (O 1s), and carbon (C 1S). As prepared Mn_2O_3 NPs' elemental composition has been examined using an X-Ray Energy Dispersive Spectrometer (EDAX). As synthesized samples, Mn-1 to Mn-3 were carried out against microbial pathogens such as *P. mirabilis* (MTCC 425), *A. hydrophila* (MTCC 12301), and *A. flavus* (MTCC 277) utilizing the Kirby-

Bauer disc diffusion approach. To find the photocatalytic activity of the prepared samples, MB dye was used as an organic pollutant.

S3 Methyl blue dye degradation via a photocatalytic oxidation mechanism

The process of photo-electrocatalytic degradation can be described as follows: under UV irradiation, 10 mg of Mn_2O_3NPs as a catalyst generates oxygen vacancies. Under the influence of an applied optical field, the photogenerated vacancy in the valence band of the Mn_2O_3 nanoparticles oxidizes OH^- ions as they travel via the linked catalyst particles to the catalyst particle–solution interface. Meanwhile, oxygen vacancies in conduction band photosynthesis are transferred to the substrate's surface in order to emit conductive UV light via catalytic particles. The mechanistic scheme describing the degradation of methylene blue dye by Mn_2O_3 is as follows:

$$Mn_2O_3 + hv\ (uv) \longrightarrow Mn_2O_3 + h^+_{(VB)} + e^-_{(CB)}$$

$$H_2O \longrightarrow H^+ + OH^-$$

$$OH^- + e^-_{(CB)} \longrightarrow OH^{\bullet -}$$

$$2O_2 + 2H_2O \longrightarrow H_2O_2 + 2OH + {}^{vacancy}O_2$$

$$Mn^{2+} / Mn^{3+} + OH \longrightarrow Mn^{3+} / Mn^{4+} + OH^- + H^+$$

$$Mn^{2+}/Mn^{3+} + OH^- \longrightarrow Mn^{3+}/Mn^{4+} + OH + H^+$$

$$Mn^{3+/}Mn^{4+} + {}^{vacancy}O_2 \longrightarrow Mn^{2+} / Mn^{3+} + O_2^{\bullet -}$$

$$OH^{\bullet -} + MB \longrightarrow CO_2 + H_2O$$

$$O_2^{\bullet -} + MB \longrightarrow CO_2 + H_2O$$

Table S1: The crystalline size, lattice strain, dislocation density and lattice parameters of the synthesized Mn_2O_3 NPs

Samples code	Precursor concentration (M)	Crystalline size (nm)
Mn-1	1	11.23
Mn-2	1.25	10.28
Mn-3	1.5	9.78

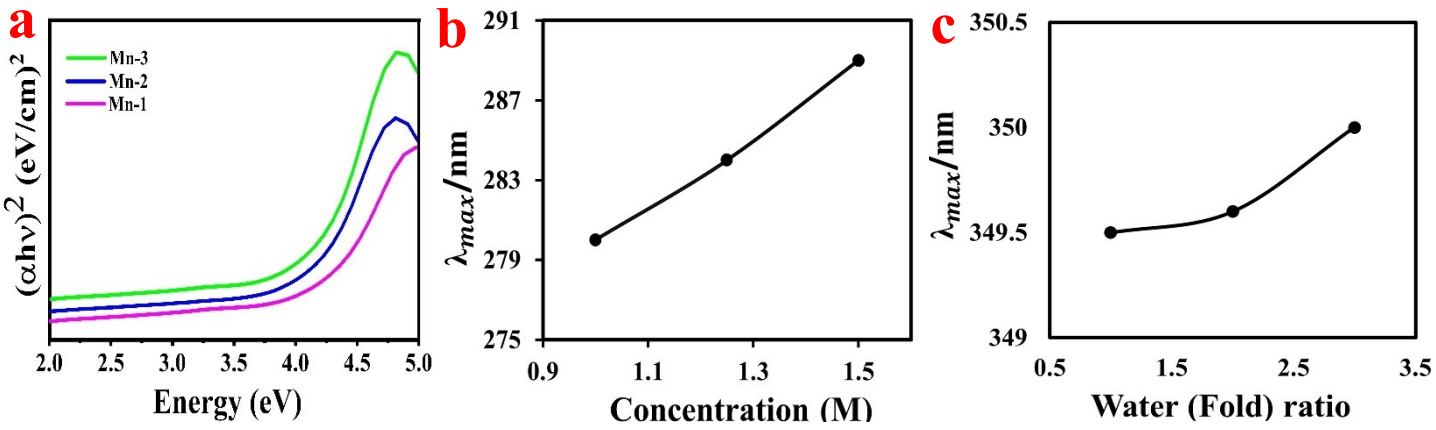

Fig. S1 (a) Tauc plot, (b) optimization of precursor concentration and (c) dilution of leaf extract

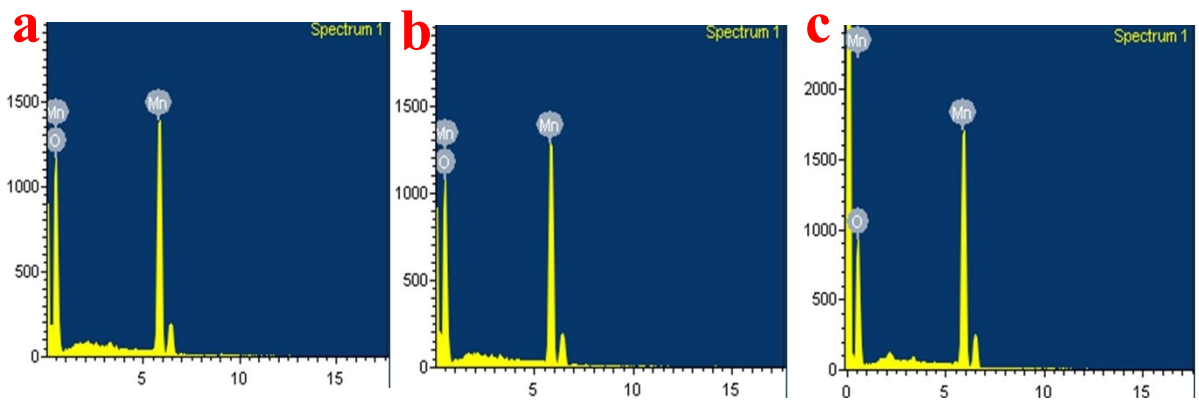

Fig. S2 EDAX spectra of prepared Mn-1 (a), Mn-2 (b), and Mn-3 (c) samples

Table S2: Elemental composition of synthesized Mn_2O_3 NPs

Elements	Samples code (%)					
	Mn-1		Mn-2		Mn-3	
	Atomic	Weight	Atomic	Weight	Atomic	Weight
Mn	37.17	67.02	37.37	67.20	47.59	75.72
O	62.83	32.98	62.63	32.80	52.41	24.28

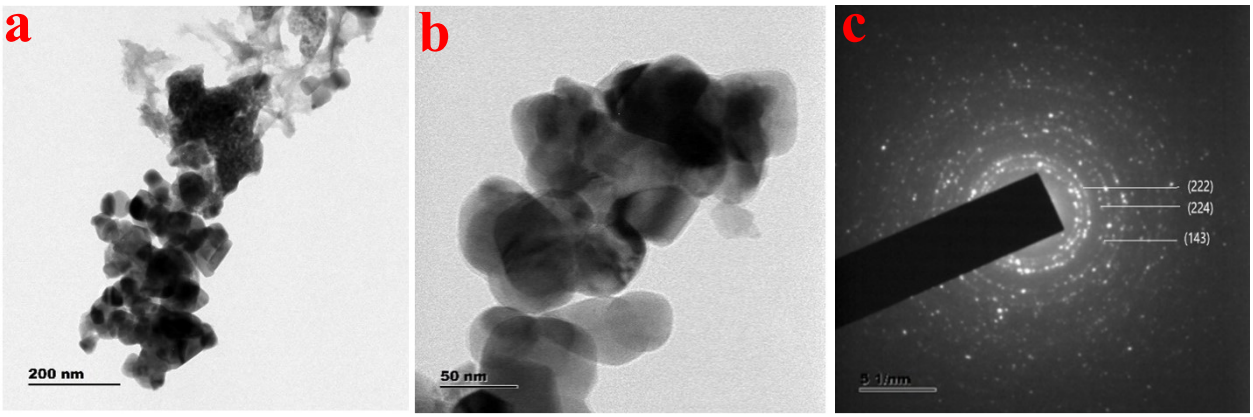

Fig. S3 (a-b) HRTEM images and (c) SAED pattern of prepared Mn-3 NPs

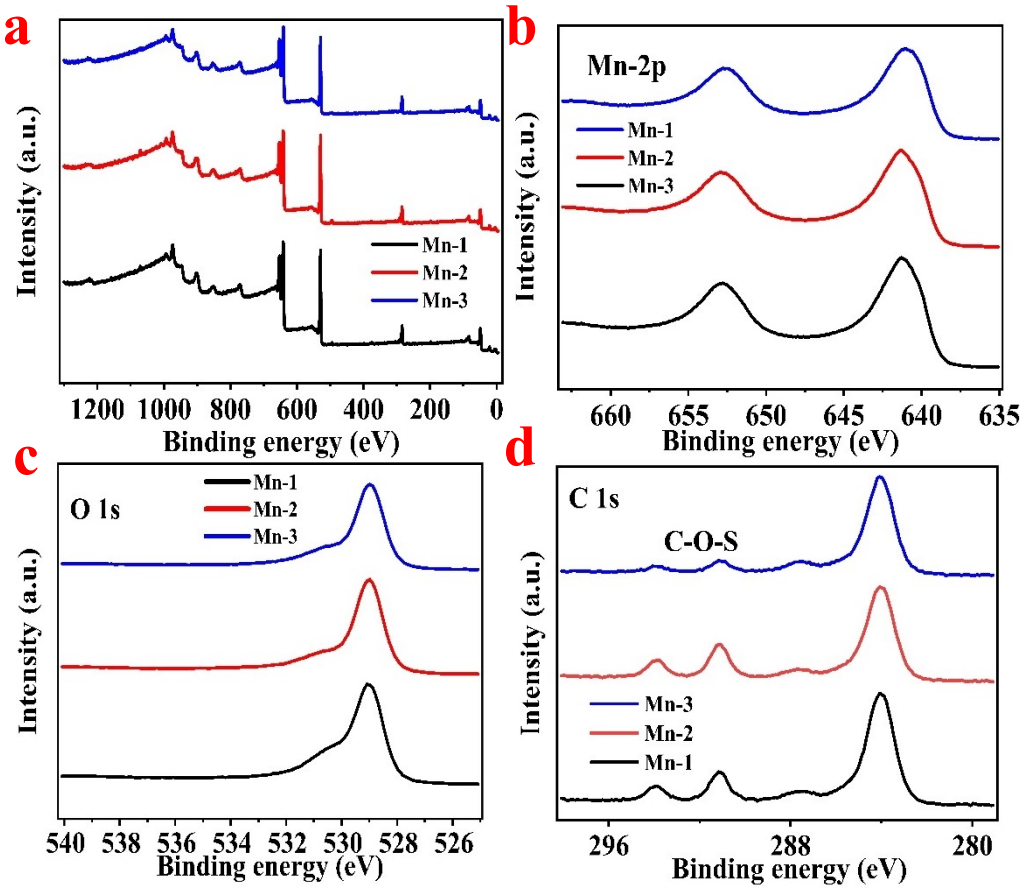
a
Intensity (a.u.)
Mn-1
Mn-2
Mn-3
1200 1000 800 600 400 200 0
Binding energy (eV)
b
Mn-2p
Mn-1
Mn-2
Mn-3
Intensity (a.u.)
660 655 650 645 640 635
Binding energy (eV)
c
O 1s
Mn-1
Mn-2
Mn-3
Intensity (a.u.)
540 538 536 534 532 530 528 526
Binding energy (eV)
d
C 1s
C-O-S
Mn-3
Mn-2
Mn-1
Intensity (a.u.)
296 288 280
Binding energy (eV)

Fig. S4 depicts the Mn-1, Mn-2, and Mn-3 samples XPS wide scan (a), Mn2p (b), O 1s (c), and C 1s (d) core spectra.

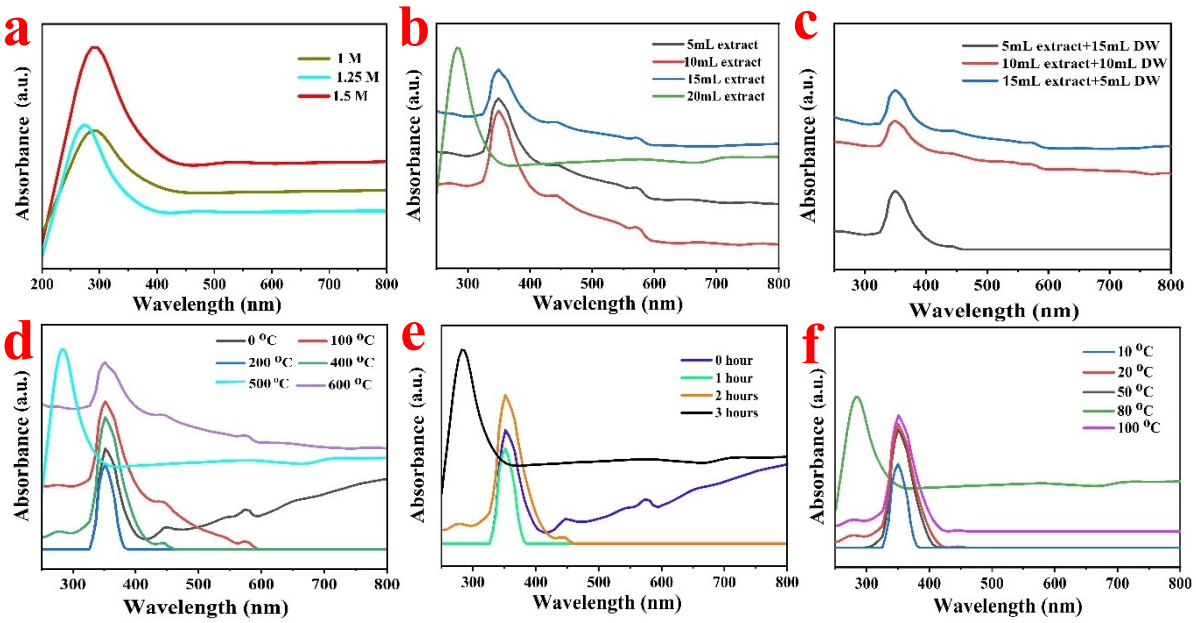
a
Absorbance (a.u.)
Wavelength (nm)
1 M
1.25 M
1.5 M
b
Absorbance (a.u.)
Wavelength (nm)
5mL extract
10mL extract
15mL extract
20mL extract
c
Absorbance (a.u.)
Wavelength (nm)
5mL extract+15mL DW
10mL extract+10mL DW
15mL extract+5mL DW
d
Absorbance (a.u.)
Wavelength (nm)
0 °C
100 °C
200 °C
400 °C
500 °C
600 °C
e
Absorbance (a.u.)
Wavelength (nm)
0 hour
1 hour
2 hours
3 hours
f
Absorbance (a.u.)
Wavelength (nm)
10 °C
20 °C
50 °C
80 °C
100 °C

Fig. S5 Optimization of UV absorption spectra of (a) precursor concentration, (b) leaf extract concentration, (c) dilution of leaf extract, (d) calcination temperature, (e) calcination time and (f) oven temperature variation

Table S3: The ZOI of prepared Mn_2O_3 NPs against the microbial pathogens

Microbial pathogen	Zone of inhibition (mm)			Control (mm)
	Mn-1	**Mn-2**	**Mn-3**	**(Amikacin)**
Proteus Mirabilis	20	20	23	21
Aeromonas hydrophilla	18	20	22	17
Aspergillus flaves	17	14	17	(**Nystatin**) 17

Table S4 Comparison of the photocatalytic degradation of various dyes in the presence of metal earth oxide to a previous work sample**.**

S. No	Catalyst	Dye	Irradiation time (min)	Conc. of dye	Conc. of catalyst (mg)	Dye degradation percentage	Reference
1	ZrO_2	MB	6 h	100 mL	20	57 %	1
2	Mn_2O_3	MB	6 h	2.5 mg	50	71 %	2
3	Ag	MB	120	100 mL	10	72 %	3
4	ZnO	MB	120	1 mM	15	63 %	4
5	PVA-ZnO/ Mn_2O_3	Acid orange-8	120	20 ppm	60	74 %	5
6	ZrO_2	MB	5 h	10 ppm	25	89 %	6
7	Pd	MB	90	10^5 M	10	81 %	7
8	Mn_2O_3	MB	120	30 ppm	10	81 %	Current

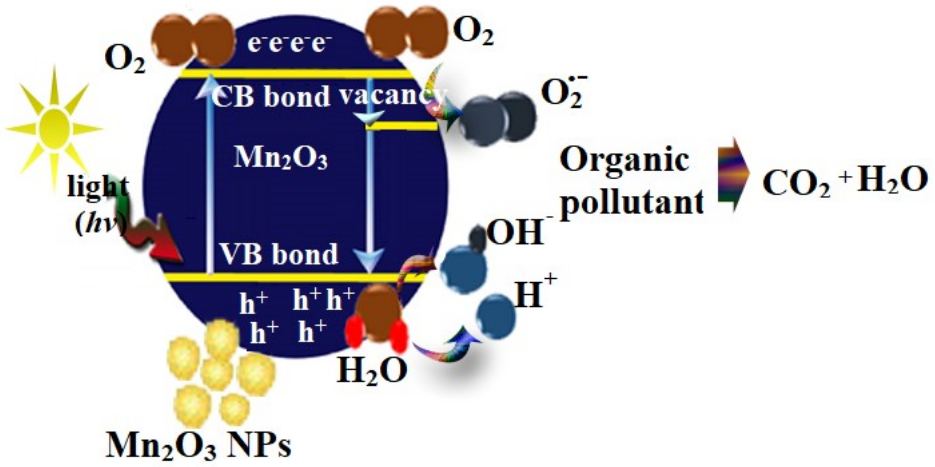

Fig. S6. demonstrate the potential photocatalytic dye degradation mechanism

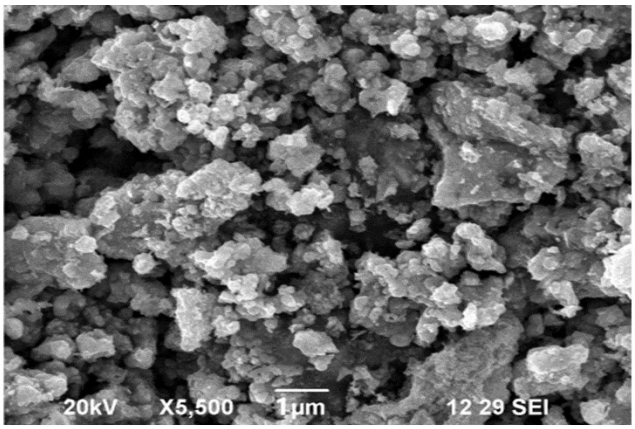

Fig. S7. SEM image describing the stability of prepared Mn-3 sample after photocatalytic dye degradation

Reference

1. Y. Yuan, Y. Wu, N. Suganthy, S. Shanmugam, K. Brindhadevi, A. Sabour, R. Shanmuganathan, Food Chem. Toxicol., 2022, 168, 113340-113348.
2. M. Pudukudy, Z. Yaakob, Journal of Nanoparticles, 2016, 2016,1-8.

3. M. Aravind, A. Ahmad, I. Ahmad, M. Amalanathan, K. Naseem, S. M. M. Mary, M. Zuber, J. Environ. Chem. Eng., 2021, 9, 104877-104906.
4. G. Madhumitha, J. Fowsiya, N. Gupta, A. Kumar, M. Singh, J. Phys. Chem. Solids, 2019, 127, 43-51.
5. B. Abebe, E. A. Zereffa, H. A. Murthy, ACS omega, 2020, 6, 954-964.
6. R. Vinayagam, B. Singhania, G. Murugesan, P. S. Kumar, R. Bhole, M. K.Narasimhan, R. Selvaraj, Environ. Res., 2022, 214, 113785-113792.
7. Y. Liang, H. Demir, Y. Wu, A. Aygun, R. N. E. Tiri, T. Gur, Y. Vasseghian, Chemosphere, 2022, 306, 135518-135528.